

Absence of diagonal force constants in cubic Coulomb crystals

Bartholomew Andrews

*TCM Group, Cavendish Laboratory, University of Cambridge, Cambridge CB3 0HE, United Kingdom and
Department of Physics, University of Zurich, Winterthurerstrasse 190, 8057 Zurich, Switzerland*

Gareth Conduit

*TCM Group, Cavendish Laboratory, University of Cambridge, Cambridge CB3 0HE, United Kingdom
(Dated: March 25, 2022)*

The quasi-harmonic model proposes that a crystal can be modeled as atoms connected by springs. We demonstrate how this viewpoint can be misleading: a simple application of Gauss' law shows that the ion-ion potential for a cubic Coulomb system has no diagonal harmonic contribution and so cannot be modeled by springs. We investigate the repercussions of this observation by examining three illustrative regimes: the bare ionic, tight-binding, and nearly-free electron models. For the bare ionic model, we demonstrate the zero elements in the force constants matrix and explain this phenomenon as a natural consequence of Poisson's law. In the tight-binding model, we confirm that the inclusion of localized electrons stabilizes all major crystal structures at harmonic order and we construct a phase diagram of preferred structures with respect to core and valence electron radii. In the nearly free electron model, we verify that the inclusion of delocalized electrons, in the form of a background jellium, is enough to counterbalance the diagonal force constants matrix from the ion-ion potential in all cases and we show that a first-order perturbation to the jellium does not have a destabilizing effect. We discuss our results in connection to Wigner crystals in condensed matter, Yukawa crystals in plasma physics, as well as the elemental solids.

The classical theory of crystal stability was extensively studied by Born in the first half of the 20th Century¹. This seminal work focused on deriving the Born stability criteria based on the elasticity constants, as well determining the scope of the Cauchy-Born rule of crystal deformation². Since this time, the topic of crystal stability has been revisited from numerous perspectives³: from the historic models of ionic matter by Born-Landé⁴, Born-Mayer⁵, and Kapustinskii⁶; the Hume-Rothery rules for metal alloys⁷; through to sophisticated quantum Monte Carlo simulations in current research^{8,9}. However, these works are based on quadratic modes, which we demonstrate can be absent from the most basic ion-ion interaction of many common crystal structures. This motivates us to revisit the stability analysis of prototypical models, which are currently of interest to the electronic structure³, plasma physics¹⁰, and astrophysics¹¹ communities.

In this paper, we study the force constants matrix with respect to atomic positions for infinite crystals in the bare ionic, tight-binding, and nearly-free electron regimes. Having observed that the ion-ion potential for cubic crystal structures has no diagonal harmonic contribution, we seek to answer the question of what repercussions this has on preferred crystal structure. By looking at a variety of crystal lattices, motivated by the elemental solids in the periodic table, we draw comparisons between specific structures. We stabilize the ionic crystal for all structures through the inclusion of electrons in our model, we study the stability transition, and use our framework to unify complementary models in the literature. We show that, using this simple yet overlooked observation, insight is gained into low-energy crystal structure relaxation.

We first introduce the underlying theory in Sec. I. We then proceed to examine the bare ionic crystal, and subsequently the tight-binding, and nearly-free electron regimes in Secs. II, III, and IV, respectively. Finally, we summarize the conclusions and implications of the results in Sec. V.

I. THEORY

We consider an infinite crystal of atoms in three-dimensions and at zero-temperature.

The Hamiltonian of the system may be written as

$$\hat{H} = \hat{T}_i + \hat{T}_e + \hat{V}_{i-i} + \hat{V}_{e-i} + \hat{V}_{e-e},$$

where \hat{T}_i , \hat{T}_e are the ion and electron kinetic energies, and \hat{V}_{i-i} , \hat{V}_{e-i} , and \hat{V}_{e-e} , are the ion-ion, electron-ion, and electron-electron contributions to the potential energy, respectively. In the tight-binding model, the kinetic energy of the nuclei is obtained by considering the confinement energy due to the presence of orthogonal harmonic wells $\sum_{i \in \{x,y,z\}} \hbar\omega_i/2$, where the eigenfrequencies ω_i are computed from the dynamical matrices. In all other models, we are solely determining instability and since the potential energy well is flat in the expansion, the kinetic energy is zero. The kinetic energy of the electrons, on the other hand, is more involved. In the tight binding model, it is split into two parts: one from confinement in a potential well and the other from tunneling. Since the energy due to confinement is effectively independent of atom positions and the energy due to confinement is exponentially small, we take the kinetic energy to be constant in our approximation. In the nearly-free electron

model, the kinetic energy takes a value directly proportional to the Fermi energy, and so again it can be taken to be constant. The three potential terms are given by the Coulomb repulsion. In the tight-binding model, the electron-electron potential energy term is further decomposed into contributions from the Coulomb repulsion of point charges and the Pauli repulsion of overlapping electron clouds (as detailed in Sec. SV E). In the nearly-free electron model, the electron density is instead given by a cosine function (presented in Sec. SVI).

Each unit cell of the crystal has an atom at the origin of the cell with position \mathbf{R}_I (upper case). There may also be additional atoms in the unit cell with displacement vectors \mathbf{r}_i (lower case) relative to \mathbf{R}_I . The general position of an atom at equilibrium may be written as $\mathbf{R}_{Ii}^0 = \mathbf{R}_I + \mathbf{r}_i$. We consider an instantaneous small and finite displacement \mathbf{u}_{Ii} of an atom in the crystal, such that the general position of an atom is given as $\mathbf{R}_{Ii} = \mathbf{R}_I + \mathbf{r}_i + \mathbf{u}_{Ii}$. The total energy of the system is then given by $E = T + \sum_{I,Jij} V(\mathbf{R}_{Ii} - \mathbf{R}_{Jj})$, where we sum over all distinct pairs.

Harmonic lattice dynamics is based on a Taylor expansion of the total energy about structural equilibrium, such that

$$E(\{\mathbf{R}_{Ii}\}) = E(\{\mathbf{R}_{Ii}^0\}) + \frac{1}{2} \sum_{I\alpha,j\beta} \Phi_{I\alpha,0j\beta} u_{I\alpha} u_{0j\beta},$$

where α, β are Cartesian directions and the adiabatic and harmonic approximations are assumed. The quantity $\Phi_{I\alpha,0j\beta}$ is known as the matrix of force constants, given as

$$\Phi_{I\alpha,0j\beta} = \left. \frac{\partial^2 E}{\partial u_{I\alpha} \partial u_{0j\beta}} \right|_{\mathbf{u}=\mathbf{0}},$$

where $J = 0$ due to translational invariance. This quantifies the stability of a crystal due to the movement of particular atoms. In periodic solids, it is common to subsequently examine the mass-reduced Fourier transform of the force constants matrix, known as the dynamical matrix, given as

$$D_{i\alpha,j\beta}(\mathbf{k}) = \frac{1}{\sqrt{m_i m_j}} \sum_I \Phi_{I\alpha,0j\beta} e^{-i\mathbf{k}\cdot\mathbf{R}_I}, \quad (1)$$

where m_i is the mass of particle i and \mathbf{k} is the linear momentum vector. The dynamical matrix is used to compute eigenmodes and definitively quantify whether a system is stable.

In 1904 Drude proposed the paradigmatic model of a crystalline solid to be atoms connected by springs, which implies that the atoms move in a harmonic potential¹²⁻¹⁴. Here we focus on the crucial contribution to this atom-atom potential, the ion-ion interaction. The Poisson equation of Gauss' theorem, for a one-component ionic lattice in the absence of any background charge, reads $\sum_{\alpha} \Phi_{I\alpha,0i\alpha} = 0$. For systems with a cubic symmetry this further implies $\Phi_{I\alpha,0i\beta} = 0$. We refer to the quantity

$\Phi_I \equiv \Phi_{I\alpha,0i\beta}$ as the diagonal force constant matrix, and the corresponding mass-reduced Fourier transform $D_{i\alpha,i\beta}$ as the diagonal dynamical matrix. We use the diagonal matrix of force constants to quantify whether a system is not stable (see Sec. SI)¹⁵. Moreover, in cases where $\Phi_{I\alpha,0i\beta} = 0$, we additionally examine the symmetry-contracted fourth-order diagonal force constant matrix, given as $\mathbf{X}_I \equiv X_{I\alpha,0i\beta}$ (see Sec. SII)¹⁶. This simple analysis shows that the diagonal matrix of force constants, as well as the diagonal dynamical matrix, are both identically zero for these cubic crystals. Since the trace of a matrix is equal to the sum of the eigenvalues, this implies that cubic systems are not (de)stabilized by the harmonic term. Furthermore, crystals without cubic symmetry will have $\Phi_{0i\alpha,0i\beta} \neq 0$ and so we expect some directions to be unstable at harmonic order by geometry. This provides strong motivation to study the repercussions of this result.

With the strategy and motivation in place, we still face the challenge of calculating the total energy. We therefore turn to three limits where we can make progress: the bare ionic crystal, and subsequently the tight-binding, and nearly-free electron models.

II. BARE IONIC MODEL

We start with the simplest system that demonstrates the concept of this paper. For the bare ionic crystal, we consider a one-component crystal of Coulomb point charges of equal sign and infinite extent. This is typical of the systems studied in plasma physics¹⁷, albeit without a background of positive charges. Working in atomic units, the Coulomb potential is $V(\mathbf{R}) = |\mathbf{R}|^{-1}$ corresponding to repulsive interactions between the point charges¹⁸. Our strategy is to determine if the crystal has a zero diagonal matrix of force constants, if so then the entire crystal is not stabilized or destabilized at harmonic order.

In Sec. II A, we discuss the background and key developments in the field of Coulomb crystals, and in Sec. II B we analyze our numerical results.

A. Background

Coulomb crystals are defined by the dominant role of the Coulomb interaction and the simple form of their constituents¹⁹. In this paper, we consider a special type of 'transient Coulomb' crystal, categorized as an unconfined and infinite, one-component system with repulsive interactions. However, the study of Coulomb crystals extends beyond this limiting case and has a history spanning over a century²⁰.

The earliest study of a one-component system was by Madelung in 1918, where he showed that an infinite array of point charges can form an ordered state²⁰. Two decades later, Wigner predicted, in his seminal paper,

that the electron jellium in metals can form a body-centered cubic crystal at sufficiently low densities^{21,22}. The subsequent numerical and experimental confirmation of Wigner crystals sparked interest in the condensed matter community, and a plethora of papers on the general theory²³⁻²⁹ and stability³⁰⁻³³ of these systems followed, including detailed quantum Monte Carlo simulations³⁴⁻⁴¹. From the plasma physics perspective on the other hand, interest in strongly coupled plasmas, i.e. plasmas where the average Coulomb energy of a particle is much greater than its average kinetic energy⁴², led to the prediction that three-dimensional, one-component Coulomb plasmas can also form a body-centered cubic crystal at sufficiently *high* densities and/or low temperatures⁴³. It was subsequently realized that these two conclusions could be reconciled as opposite density limits of the same problem⁴⁴. All of these models, however, include a homogeneous positive background of charges to stabilize the system. Indeed, there are two ways to stabilize a repulsive Coulomb crystal: a homogeneous oppositely-charged background, or confinement¹⁹.

Work on confined plasmas has been performed in a variety of contexts⁴². Most notably, the structure and Madelung energy⁴⁵, as well as the melting of ordered states⁴⁶ in spherical Coulomb crystals has been studied in the last thirty years. These systems can also be probed and manipulated experimentally using ions confined to Penning¹⁷ or Paul⁴⁷ traps, with motivation provided by the recent discovery of crystalline plasmas of dust particles in astrophysics¹¹; as well as the industrial success of quantum dot technology⁴⁸. For all of these confined systems, however, the resulting crystal structure is strongly dependent on the shape of the trap⁴⁶. Therefore, no general statements can be made about the equilibrium structure.

In this section, we study the instability of unconfined Coulomb crystals, which we stabilize in later sections through the inclusion of an oppositely-charged background.

B. Analysis

We first calculate the total energy of a lattice of ions. We examine the Bravais lattices: simple cubic (cub), body-centred cubic (bcc), and face-centred cubic (fcc). Additionally, we study the diamond (dia) lattice structure, from the fcc family, separately, as it is of special interest due to its extreme material properties, such as hardness and thermal conductivity. We also include the hexagonal close-packed (hcp) and double hexagonal close-packed (dhcp) structures in our analysis, from the hexagonal Bravais lattice family, due their ubiquity in nature (see Sec. SIII).

In order to perform the summation over lattice sites in this section we use a rotationally-symmetric summation scheme. We start by defining all unit cells with an atom at the origin and then incrementally add atoms in

Crystal	$a\Phi_0^{i-i}$	${}_{i-i}\hat{\mathbf{m}}_2$	${}_{i-i}\hat{\mathbf{m}}_2^T \cdot (a\Phi_0^{i-i}) \cdot {}_{i-i}\hat{\mathbf{m}}_2$
C	$\mathbf{0}$	$-$	0
H	$-\frac{k}{2} \begin{pmatrix} 1 & 0 & 0 \\ 0 & 1 & 0 \\ 0 & 0 & -2 \end{pmatrix}$	$\pm\hat{\mathbf{e}}_z$	$k_{\text{hcp}} = -0.33$ $k_{\text{dhcp}} = -0.8$

TABLE I. Diagonal matrices of force constants and minimizing directions for the ion-ion interaction expansion about equilibrium, at second order with lattice spacing, a . The cubic crystals are denoted by $C \in \{\text{cub, bcc, fcc, dia}\}$ and the hexagonal crystals by $H \in \{\text{hcp, dhcp}\}$. Φ_0 is the Hessian; $\hat{\mathbf{m}}_2$ is the normalized eigenvector corresponding to the lowest eigenvalue of the Hessian; and $\hat{\mathbf{m}}_2^T \cdot \Phi_0 \cdot \hat{\mathbf{m}}_2$ is the projection of the Hessian in the minimizing direction. All values are given to the precision up to which they have converged, or three significant figures, whichever is lower.

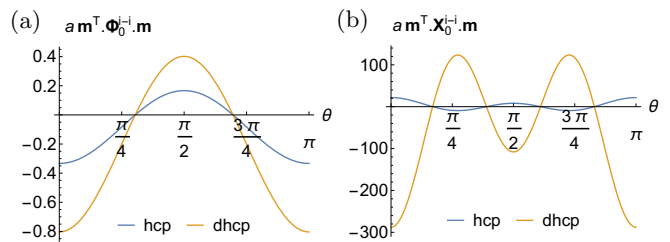


FIG. 1. Angular variation in the inner product of the matrices of force constants with a direction vector \mathbf{m} at $\phi = \pi/2$ and unit radius, in units of a^{-1} . Plots are shown for the (a) second-order, and (b) fourth-order terms for the hcp and dhcp crystal structures. Note that the inner product of the fourth-order diagonal matrices of force constants is azimuthally symmetric for these systems. The minimizing directions are recorded in Tables I & II.

concentric shells. We compute this summation until convergence to the desired precision. The full details of the numerical model are discussed in Sec. SIV of the Supplementary Material.

The diagonal matrices of force constants, directions of greatest instability, and minimal eigenvalues for these crystals are shown in Table I. In this model, the cubic systems (cub, bcc, fcc, dia) have no diagonal harmonic term in their potential energy expansion, which renders the derivative test inconclusive. The hexagonal systems (hcp, dhcp) have indefinite diagonal force constant matrices, which implies the system is at a saddle point. We see that the system is stable to diagonal perturbations in the xy-plane, but most unstable to diagonal perturbations in the z-direction, as illustrated in Fig. 1a. The dhcp system is more unstable than the hcp system with this metric due to the higher density of ions.

Having found that the cubic crystal stability test is inconclusive at second order, we turn to a higher-order expansion. An analogous table for the fourth-order diagonal matrices of force constants is shown in Table II⁴⁹. At this order, the cubic systems do not have vanishing

Crystal	$a\mathbf{X}_0^{i-i}$	${}_{i-i}\hat{\mathbf{m}}_4$	${}_{i-i}\hat{\mathbf{m}}_4^{\circ 2\text{T}} \cdot (a\mathbf{X}_0^{i-i}) \cdot {}_{i-i}\hat{\mathbf{m}}_4^{\circ 2}$
cub	$74.6 \begin{pmatrix} 1 & -1.5 & -1.5 \\ -1.5 & 1 & -1.5 \\ -1.5 & -1.5 & 1 \end{pmatrix}$	$\frac{1}{\sqrt{3}}(\pm\hat{\mathbf{e}}_x \pm \hat{\mathbf{e}}_y \pm \hat{\mathbf{e}}_z)$	-49.7
bcc/fcc/dia	$k \begin{pmatrix} 1 & -1.5 & -1.5 \\ -1.5 & 1 & -1.5 \\ -1.5 & -1.5 & 1 \end{pmatrix}$	$\{\pm\hat{\mathbf{e}}_x, \pm\hat{\mathbf{e}}_y, \pm\hat{\mathbf{e}}_z\}$	$k_{\text{bcc}} = -74.6$ $k_{\text{fcc}} = -181$ $k_{\text{dia}} = -2570$
hcp	$8.1 \begin{pmatrix} 1 & 1 & 0 \\ 1 & 1 & 0 \\ 0 & 0 & 0 \end{pmatrix} + 21.6 \begin{pmatrix} 0 & 0 & -1.5 \\ 0 & 0 & -1.5 \\ -1.5 & -1.5 & 1 \end{pmatrix}$	$\theta = 0.857, \pi - 0.857$	-9.3
dhcp	$-108 \begin{pmatrix} 1 & 1 & 0 \\ 1 & 1 & 0 \\ 0 & 0 & 0 \end{pmatrix} - 288 \begin{pmatrix} 0 & 0 & -1.5 \\ 0 & 0 & -1.5 \\ -1.5 & -1.5 & 1 \end{pmatrix}$	$\pm\hat{\mathbf{e}}_z$	-288

TABLE II. Diagonal force constant matrices and minimizing directions for the ion-ion interaction expansion about equilibrium, at fourth order, with the same conventions as Table I. Fourth-order matrices are symmetry contracted as described in Sec. SII.

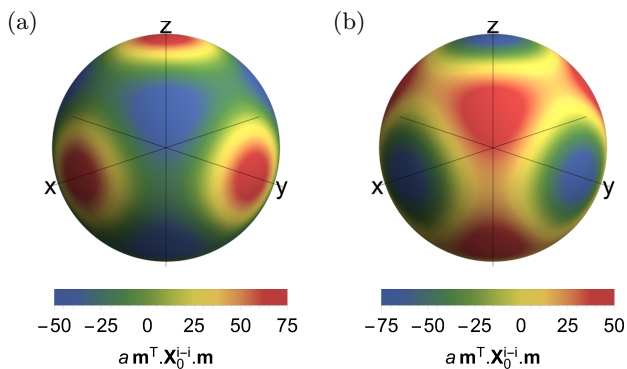


FIG. 2. Angular variation in the inner product of the fourth-order diagonal matrices of force constants with a direction vector \mathbf{m} at unit radius, in units of a^{-1} . Plots are shown for the (a) cub, and (b) bcc crystal structures. The plots for the fcc and dia crystal structures have an identical form to (b) with different scales. The scales and minimizing directions are recorded in Table II.

contributions, instead they demonstrate a fourth-order instability. Note that the form of the fourth-order matrices is similar in each case, with a varying pre-factor. Plots of the angular variation of these fourth-order matrices are shown in Fig. 2. As for the hexagonal systems at second order, the system is again at a saddle point. In this case, the configuration is stable to perturbations in the Cartesian basis directions for cub; and in the diagonal directions for bcc, fcc and dia crystals, and visa versa. For completeness, we show that the fourth-order matrices for the hexagonal systems are also indefinite, as shown in Fig. 1b. In the dhcp case, the minimizing directions are again $\pm\hat{\mathbf{e}}_z$, whereas for the hcp system the most unstable directions have now shifted to $\theta = 0.857, \pi - 0.857$. The angular variation for the hexagonal systems is rotationally symmetric about the z-axis, since the x- and y-eigenvalues are the same. Note that since higher-order (in)stabilities are always weaker than lower orders, it is unnecessary to examine the higher-order terms for these

hexagonal systems. As seen for the second-order case, the magnitude of the instabilities is determined by the ion density.

The lack of a diagonal harmonic contribution to the energy in cubic systems appears to contradict the 1904 quasi-harmonic model for a crystal of atoms connected by springs¹²⁻¹⁴. However, as stated before, it is a natural consequence of Gauss' theorem ($\partial_{xx} + \partial_{yy} + \partial_{zz}$) $V_{i-i} = 0$. In a system with cubic symmetry all terms in Gauss' theorem must be identical so each must be zero, $\partial_{ii}V = 0$. Furthermore, the entire diagonal dynamical matrix is zero for this infinite system. In systems without cubic symmetry, we can say that if in some direction the second derivative is positive, then in others it must be negative to satisfy Gauss' theorem, and so will never be stable by geometry. The changing sign in the fourth-order derivative in cubic systems is expected as Gauss' theorem requires the net electron flux through a closed surface to be zero, so positive contributions must be counterbalanced by negative contributions. We therefore deduce that it is inevitable that crystalline solids are not stabilized at any order by contributions from the ion-ion potential.

Note that in this section we have considered a one-component ionic crystal without a neutralizing background to show that cubic structures have the weakest (fourth-order) instability. In Sec. IV we will show that if a constant neutralizing background is introduced, this would provide a quadratic restoring potential for the ions, which would compensate for this instability. This holds even for non-cubic systems, since it can be shown that the stabilizing contribution to the dynamical matrix from the constant uniform background is greater than the destabilizing contribution from the purely repulsive ionic crystal.

III. TIGHT-BINDING MODEL

We found that the bare crystal of ions is not stable and so, motivated by the need to stabilize the system, we now consider the simplest model to include electrons to

bind the ions: the tight-binding model. The electrons are tightly bound to each nucleus with a spherical effective charge density parameterized by core and valence orbital radii.

We start by analyzing the model and phase diagram in Sec. III A, and then discuss the interpretation in Sec. III B.

A. Analysis

In the tight-binding approximation, the electrons are situated directly on top of and nearby to the ions. We consider ions that have only spherically symmetric (s-type) orbitals, with the electron density distribution:

$$\rho_{\text{E}}(\mathbf{r}; c, a_e) \propto \frac{1}{1 + \exp\left(\frac{2(|\mathbf{r}|-c)}{a_e}\right)},$$

where the normalization factor to give net charge neutrality is given in Sec. SV A 1 of the Supplementary Material. Here \mathbf{r} denotes the displacement of the electron relative to the origin of its associated ion, and c, a_e characterize the core and valence orbital radii, respectively. The factor of two ensures that the associated wavefunction, defined by $\rho = |\Psi|^2$, reduces to the hydrogenic atom solution, $\sim \exp(-|\mathbf{r}|/a_e)$, in the extreme tight-binding approximation: $c \ll a_e \ll a$. We choose this form of the electron orbital density³⁹, because it is analytically well behaved for the required derivation and has the correct scaling behavior (see Sec. SV A 1). Throughout our calculations, we work to leading order in the tight-binding approximation. In practice, this implies results up to first order in the small core radial parameter (c/a_e) and second order in the valence radial parameter (a_e/a).

As mentioned in Sec. I, we calculate the kinetic energy of the ions based on the presence of orthogonal harmonic wells, such that $\sum_{i \in \{x,y,z\}} \hbar\omega_i/2$, where ω_i are computed from the dynamical matrix (Eq. 1)⁵⁰. We calculate the ion-ion, electron-ion, and electron-electron contributions to the potential energy based on the electron orbital ansatz up to the approximations detailed above. We subsequently add on the contribution to the energy due to the Pauli repulsion of the overlapping electron orbitals, evaluated at the optimal effective radius of atoms in a spherical packing. Finally, we relax the crystal structure to find the optimal lattice constant, a . We perform the calculation for each of the crystal structures: cub, bcc, fcc, dia, hcp, and dhcp. For both the kinetic and potential energies, we use the same rotationally-symmetric summation scheme for the crystal introduced in Sec. II. The details of the numerical model are discussed in Sec. SV of the Supplementary Material.

In Fig. 3, we show the phase diagram of the stable crystal structures with the lowest energy out of the cub, bcc, fcc, dia, hcp, and dhcp lattices. We note that all of the crystal structures are stable with respect to their dynamical matrices in this model and so the preferred crys-

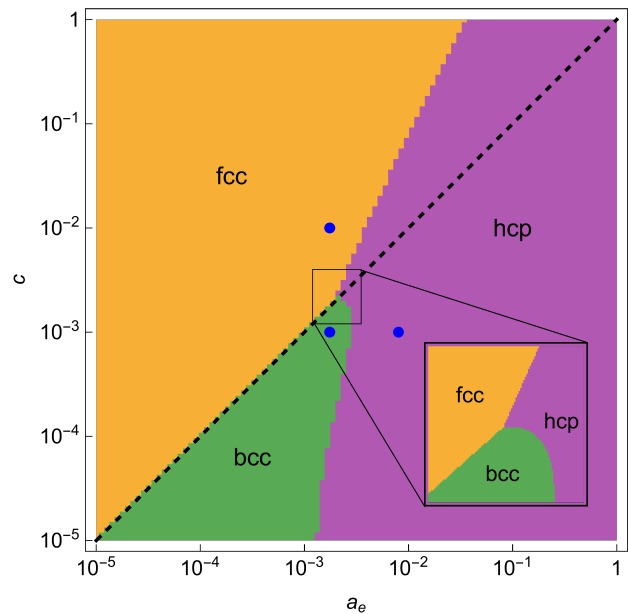


FIG. 3. Phase diagram of the lowest-energy crystal structure out of {cub, bcc, fcc, dia, hcp, dhcp} at the optimum lattice constant, summed out to eight shells. The black line separates the valid region for the tight-binding model: the lower right-hand triangle at $c < a_e$. The blue points, $\{(1.75 \times 10^{-3}, 10^{-2}), (1.75 \times 10^{-3}, 10^{-3}), (8 \times 10^{-3}, 10^{-3})\}$, are analyzed in Fig. 4. Inset: Higher-resolution plot of the region enclosed by the black square, highlighting the tricritical point. The diagrams are plotted to a resolution of 100^2 points.

tal structure is determined by the total energy hierarchy. Out of the six crystal structures considered, the hcp, fcc, and bcc structures are found to be the preferred phases. We present a higher-resolution close-up of the tricritical point in the inset of Fig. 3 to analyze the features of interest. The tricritical point is at $(a_e, c) = (2.04, 2.13) \times 10^{-3}$ with three transition lines: fcc-bcc at $c \propto a_e$; fcc-hcp at $c \propto a_e^{2.5}$; and bcc-hcp at $c = 2.13 \times 10^{-3}$ in the vicinity of the tricritical point. Since all phase transitions between allotropes of crystal structures are first order, the tricritical point is valid with respect to the vertex rule. Note that other than the restriction imposed by the tight-binding approximation, in this context $c \lesssim a_e$, the phase diagram may be extended in both directions.

Now that we have constructed the phase diagram, we verify the convergence of our calculations. Figure 4 shows a detailed analysis of the blue points depicted in Fig. 3. Most importantly, we see from plots of the total energy against number of shells in the summation, that convergence is reached at approximately five shells. Therefore, we plot the phase diagram by summing over eight shells, deep into the converged region. We consistently observe that {bcc, fcc, hcp} forms the energetically favorable subset of crystal structures.

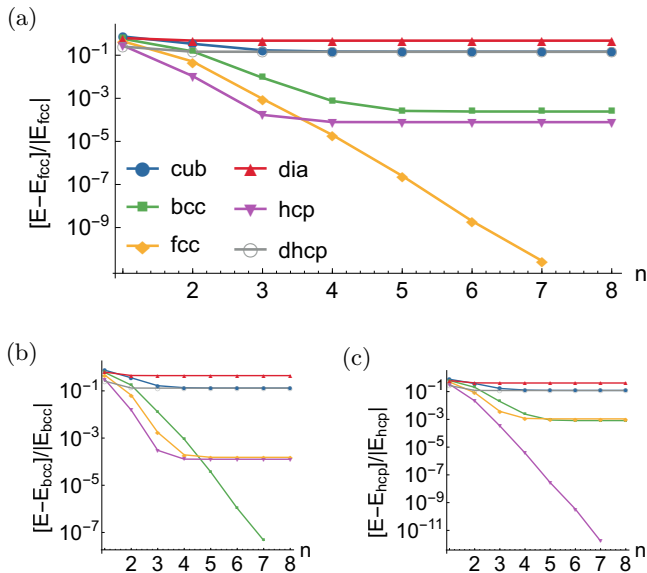


FIG. 4. Detailed analysis of the blue points depicted in Fig. 3, such that (a) is at $(a_e, c) = (1.75 \times 10^{-3}, 10^{-2})$, (b) is at $(1.75 \times 10^{-3}, 10^{-3})$, and (c) is at $(8 \times 10^{-3}, 10^{-3})$. The plots show the fractional deviation of the energies from the lowest energy value at eight shells, $[E - E_{c.s.}(n=8)]/|E_{c.s.}(n=8)|$, against the number of shells summed over, n .

B. Discussion

In this section, we progressed from the ionic crystal in Sec. II by introducing tightly-bound electrons to stabilize the system. Three phases emerged with noticeably lower energy: hcp, bcc, and fcc. Each is the ground state in different limits, and have been separately noted before, hence the tight-binding model presented allows us to reconcile previous findings in a unified framework. We now discuss how these phases emerge in the three separate limits of our tight binding model.

It has been known for a long time that three-dimensional Coulomb crystals have a bcc symmetry⁴³, where the term ‘‘Coulomb crystal’’ in plasma physics refers to strongly-coupled charged particles with a neutralizing background¹⁹. In the tight-binding limit ($c \ll a_e \ll a$), this is effectively equivalent to the system presented in Fig. 3. The particle interactions are Coulomb-like, since the effect of the well is still minimal, and the presence of the electrons provides the neutralizing background, albeit highly concentrated around the ions. Therefore, it is unsurprising that we see the same bcc ground state crystal structure. This also has parallels to a Wigner crystal, where the decay of the electronic wavefunction is sufficiently slow to stabilize the crystal²¹.

As soon as we move into the region where $c > a_e$ we modify the effective interaction through screening. In this region we observe the behavior of screened Coulomb charges, and when $c \gg a_e$ and $c \gg a$ we observe the nearly-free electron model. Indeed, it has been shown by Hamaguchi et al.⁵¹ that three-dimensional Yukawa

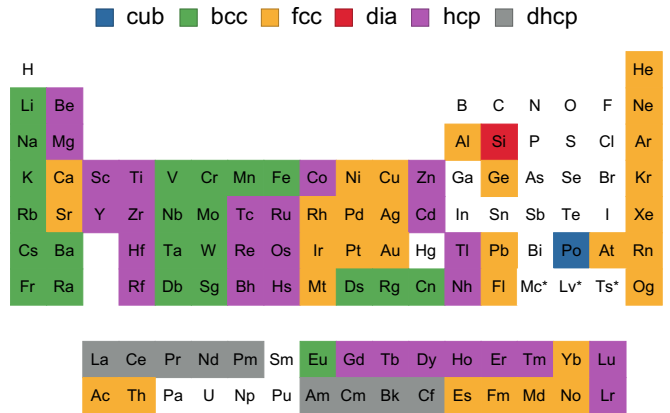


FIG. 5. The periodic table of elements labeled according to the crystal structure of their thermodynamically most stable allotrope⁵². The white cells correspond to elements with a crystal structure that is not in the set {cub, bcc, fcc, dia, hcp, dhcp}. The crystal structures of elements marked with an asterisk is not known.

crystals have a bcc and fcc phase. They show that there exist two solid phases for the Yukawa crystal: bcc at small screening parameter and a transition to fcc when the screening parameter is increased, which corresponds to moving vertically upwards in our phase diagram.

In addition to these extreme limits, our model provides insight into the transition from extreme matter to real materials. From Fig. 3, we can see that as a_e is increased, that is the valence electron radius is increased and the tight-binding approximation is relaxed, the hcp structure is energetically favorable, for both $c < a_e$ and $c > a_e$. This shows that in many materials the crystal lattice begins to favor high symmetry and packing factor. The limit applies to many of the Lanthanides and Actinides that are in the tight-binding regime⁵³. Moreover, as shown in Fig. 5 and discussed in Sec. SIII of the Supplementary Material, the hexagonal structure is the most common Bravais lattice in the periodic table. More generally, the vast majority of the periodic table is composed of the bcc, fcc, and hcp crystal structures⁵⁴, identified here are the three most energetically favorable structures.

IV. NEARLY-FREE ELECTRON MODEL

In contrast to the tight binding model, where the Bohr radii of the atoms are much smaller than the inter-atomic spacing, we now consider the opposite ‘‘nearly-free electron’’ limit, where the Bohr radii mostly overlap. This is applicable to a variety of simple metals in the periodic table, and particularly the Alkali metals. In the weak binding, or nearly-free electron model, we perform first-order perturbation theory about the jellium model, where the electron density is uniform. In this section we consider an ideal crystal, which is infinitely periodic in

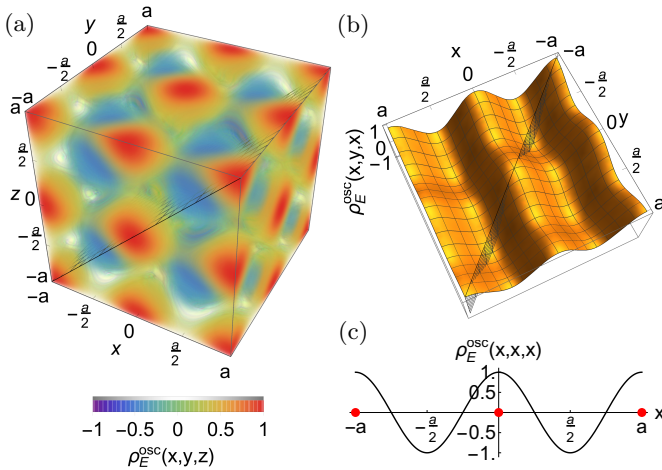


FIG. 6. (a) Three-, (b) two-, and (c) one-dimensional plots of the oscillatory part of the electron cloud density, $\rho_E^{\text{osc}}(x, y, z) = [\cos(kx) + \cos(ky) + \cos(kz)]/3$ with $k = 2\pi/a$, for the simple cubic lattice in the nearly-free electron model. (a) Color and opacity both denote the magnitude of $\rho_E^{\text{osc}}(x, y, z)$. (b) Plot of the meshed cross-section depicted in (a), through the density extrema. (c) Plot of the meshed cross-section depicted in (b), through the density extrema. The red points illustrate the positions of the ions.

space. Our strategy is to focus on the ion motions found in Sec. II to be not stable, and then investigate whether the electron cloud can compensate for this. The details of the electron cloud densities in this model are presented in Sec. SVI of the Supplementary Material.

The nearly-free electron model comprises a lattice of ions with Coulomb repulsion, as studied in Sec. II, together with an oscillatory and near-uniform electron cloud density, ρ_E . In accordance with first-order perturbation theory, this electron cloud density may be split into two parts, $\rho_E = \rho_E^{\text{cst}} + \rho_E^{\text{osc}}$, with ρ_E^{cst} corresponding to the constant jellium-like density, and ρ_E^{osc} corresponding to the oscillatory density due to the electron-ion interaction and the geometry of the ionic lattice. An example of the oscillatory electron cloud density for the simple cubic lattice is shown in Fig. 6. In each case, we ensure that the density range is normalized such that $\max(\rho_E^{\text{osc}}) = u$, where u is the oscillation strength, and that the integral of ρ_E^{osc} over a unit cell is equal to zero.

In order to calculate the total diagonal force constant matrix, we proceed as before by summing the ion-ion, electron-ion, and electron-electron contributions. For the ion-ion contribution, we take results directly from Sec. II. Note that when performing the summation over shells for the ion-ion contribution, the zeroth-order contribution to the energy is divergent, whereas the matrix of force constants converges as demonstrated in Table I. In fact, there are divergent zeroth-order contributions for the electron-ion and electron-electron contributions too, corresponding to the jellium-like term in the electron density. These divergent terms cancel, similar to the obser-

vation in Sec. III. However, we gain additional insight by directly calculating the diagonal force constants matrix in each case. The constant electron-ion contribution to the diagonal force constants matrix must satisfy $\sum_{\alpha} \Phi_{I\alpha, 0i\alpha}^{e-i, \text{cst}} = 4\pi\rho_E^{\text{cst}}$ by Poisson's law. The uniform neutralizing background stabilizes any crystal with respect to diagonal force constants and its contribution is summarized in Table III.

The oscillatory electron-ion contribution, $E_{e-i}^{\text{osc}}(\mathbf{u}) = -2 \sum_I \int V_i(\mathbf{R}_I - \mathbf{u} + \mathbf{r}_e) \rho_E^{\text{osc}}(\mathbf{r}_e) d\mathbf{r}_e$, may be simplified by noting that all ions are equivalent and so we can focus on the ion at the origin. Subsequently calculating the energy per atom allows us to drop the summation over ions and write

$$E_{e-i}^{\text{osc}}(\mathbf{u}) = -2 \int V_i(-\mathbf{u} + \mathbf{r}_e) \rho_E^{\text{osc}}(\mathbf{r}_e) d\mathbf{r}_e, \quad (2)$$

where V_i is given by the Coulomb potential and the oscillatory part of the electron density is approximated by a cosine function (see Sec. SVI).

Finally, for the electron-electron contribution, $E_{e-e} = \sum_I \iint V_e(\mathbf{R}_I - \mathbf{u} + \mathbf{r}_e - \mathbf{u}_e) \rho_E(\mathbf{r}_e) \rho_E(\mathbf{u}_e) d\mathbf{r}_e d\mathbf{u}_e$, we may drop the summation by the same argument. Note also that the electron potential does not depend on the displacement of the central atom. Hence, excluding the zeroth-order term and working to first-order in the perturbation strength, we may write the oscillatory contribution to the electron-electron energy as

$$E_{e-e}^{\text{osc}} = 2\rho_E^{\text{const}} \int_{\mathbf{r}_e \in \text{unit cell}} \int_{\mathbf{u}_e \in \mathbb{R}^3} V_e(\mathbf{r}_e - \mathbf{u}_e) \rho_E^{\text{osc}}(\mathbf{u}_e) d\mathbf{u}_e d\mathbf{r}_e, \quad (3)$$

where the factor of two is from the addition of both cross terms, and V_e is again given by the Coulomb potential. For all structures the positive and negative regions of the oscillatory electron density ρ_E^{osc} cancel and therefore the oscillatory electron-electron contribution is zero, $E_{e-e}^{\text{osc}} = 0$.

The summation of the leading-order terms from Sec. II, the jellium contribution, as well as the oscillatory contributions from Eqs. 2 and 3 yields the total energy, the diagonal matrix of force constants, and hence an instability discriminant.

The harmonic energy contributions for the cub, bcc, fcc, dia, hcp, and dhcp crystal structures is summarized in Table III. We note that all of the electron-ion contributions are positive at this order. We can see that the cubic structures all have isotropic matrices, whereas the hexagonal structures are only isotropic in the xy -plane, as expected by symmetry.

For all of the crystals considered, the electron-ion term from the constant electron background alone is sufficient to counterbalance the corresponding ion-ion term. The oscillating electron background provides additional stability for these diagonal terms. We note that, for the complete stability hierarchy in the nearly-free electron system, the dynamical matrices need to be studied, as well as additional effects, such as the electron per atom

Crystal	$a(\Phi_0^{e-i,cst} + \Phi_0^{e-i,osc})$
C	$\frac{4\pi}{3} (k + \sqrt{2\pi\tilde{u}}) \mathbf{I}$
hcp	$\frac{4\sqrt{2}\pi}{41} (1 + \sqrt{\pi\tilde{u}}) \begin{pmatrix} 16 & 0 & 0 \\ 0 & 16 & 0 \\ 0 & 0 & 9 \end{pmatrix}$
dhcp	$\frac{4\sqrt{2}\pi}{697} (2 + \sqrt{\pi\tilde{u}}) \begin{pmatrix} 218 & 0 & 0 \\ 0 & 218 & 0 \\ 0 & 0 & 261 \end{pmatrix}$

TABLE III. Electron-ion contributions to the diagonal force constants matrix in the nearly-free electron model. The cubic crystals are denoted by $C \in \{\text{cub}, \text{bcc}, \text{fcc}\}$. The prefactors for the constant electron-ion contributions for cubic systems are $\{k_{\text{cub}}, k_{\text{bcc}}, k_{\text{fcc}}\} = \{1, 2, 4\}$. \mathbf{I} and \tilde{u} denote the identity matrix and dimensionless oscillation strength, respectively.

concentration and the band lowering at the Brillouin zone boundaries^{55,56}.

In the empty lattice approximation ($\tilde{u} \approx 0$), we find that cubic systems have positive diagonal harmonic terms of larger magnitude than hexagonal systems, and in particular the fcc structure has the largest diagonal harmonic term. This potentially concurs with the nearly-free limit $c \gg a_e$ and $c \gg a$ of the tight-binding model. Furthermore, this matches observations in the periodic table, not only for the quintessential empty lattice case study: aluminium⁵⁷, but also nickel, copper, silver, and gold⁵⁸ – all of which have an fcc structure.

In this section, we have shown that, considering the diagonal harmonic terms, all ionic crystals are counterbalanced with the addition of constant neutralizing background, and that a first-order oscillatory component to the background does not have a destabilizing effect. The fcc lattice has the largest such term, in agreement with many itinerant elemental solids.

V. CONCLUSION

In this paper, we have studied lattice instability of unconfined crystal structures at zero-temperature in the bare ionic, tight-binding, and nearly-free electron models. We analyzed the diagonal matrices of force constants to expose instability and focused on the $\{\text{cub}, \text{bcc}, \text{fcc}, \text{dia}, \text{hcp}, \text{dhcp}\}$ structures due to their prevalence in nature and distinctive properties.

In Sec. II, we studied a bare one-component system of point Coulomb charges. First, we reviewed the history of the field, and noted that the bcc structure is special for being the stable crystal structure for both the low density Wigner crystal and the high density Coulomb crystal in the one-component plasma model. We then demonstrated that in this regime, cubic crystal structures have no diagonal contribution to the matrix of force constants at quadratic order but instead an instability at fourth order, whereas all other crystal structures have an instabil-

ity at second order. This is counter to the paradigmatic quasi-harmonic model of ions connected by springs¹²⁻¹⁴. These findings motivated us to continue and examine the preferred structure as we permit background charges to stabilize the system.

In Sec. III, we stabilized the lattice through the addition of electron orbitals. We constructed a tight-binding model, and found that in the extreme tight-binding limit, the bcc structure is the most stable, as suspected from the results and discussion in Sec. II. We also showed that if we tune the parameters to increase screening in our pseudopotential model of the nucleus and approach the nearly-free electron limit, the fcc structure is the stable ground state. This agrees with theoretical studies of unconfined three-dimensional Yukawa crystals in the literature. Finally, we report the second dominant phase to be hcp as we tune away from tight binding, which accords to trends in the periodic table. The use of the tight-binding model with the systematic analysis of terms has allowed us to combine the emergence of these three separate phases into a single framework.

In Sec. IV, we briefly examined the instability of crystal structures in the opposite limit, nearly-free electrons, which is representative of many common metals. In this model, we found that the instability of every crystal structure is counterbalanced with the addition of a constant neutralizing background, and that a first-order oscillatory perturbation to the background does not have a destabilizing effect. We note here that a formal stability analysis would require the complete dynamical matrix. The most stable crystal structure in the empty lattice approximation according to this metric is fcc, agreeing not only with a limit of the tight-binding model, but also with several structures observed in the periodic table.

By investigating three simple cases, motivated by the absence of diagonal force constants in cubic Coulomb crystals, this paper highlights the connections and limitations of paradigmatic crystal models for stability. For many real materials, there are a plethora of important effects that need to be taken into consideration to determine the optimal lattice structure e.g. temperature effects, the shape of the atomic orbitals, the precise band structure, or the van der Waals interaction, which leaves scope for future work. However, we have identified minimal models to illustrate the interesting physical effects at play, shown how the tight-binding and nearly-free electron theories may be linked, and connected historical theories of crystal structures at low energies. We hope that this closer look at the energies and force constants for these three models will instill a greater appreciation and understanding of the requirements for crystal stability, as well as its connection with lattice geometry.

ACKNOWLEDGMENTS

We thank Emilio Artacho, Edward Linscott, Chris Pickard, Daniel Rowlands, Beñat Mencia Uranga,

Claudio Castelnovo, Yu Yang Fredrik Liu, and Pablo López Ríos for useful discussions. B.A. acknowledges support from the Engineering and Physical Sciences Research Council under Grant No. EP/M506485/1

and the Swiss National Science Foundation under Grant No. PP00P2_176877. G.J.C. acknowledges support from the Royal Society. Open access to the data in this paper is available at the DSpace@Cambridge repository.

- ¹ M. Born, *Math. Proc. Cam. Philos. Soc.* **36**, 160172 (1940).
- ² J. Ericksen, *Math. Mech. Solids* **13**, 199 (2008).
- ³ G. Grimvall, B. Magyari-Köpe, V. Ozoliņš, and K. A. Persson, *Rev. Mod. Phys.* **84**, 945 (2012).
- ⁴ D. Brown, *The Chemical Bond in Inorganic Chemistry* (Oxford University Press, Oxford, UK, 2002).
- ⁵ M. Born and J. E. Mayer, *Z. Phys.* **75**, 1 (1932).
- ⁶ A. F. Kapustinskii, *Q. Rev. Chem. Soc.* **10**, 283 (1956).
- ⁷ W. Hume-Rothery and H. Powell, *Zeitschrift für Kristallographie* **91**, 23 (1935).
- ⁸ K. P. Driver, R. E. Cohen, Z. Wu, B. Militzer, P. L. Ríos, M. D. Towler, R. J. Needs, and J. W. Wilkins, *Proc. Natl. Acad. Sci. U.S.A.* **107**, 9519 (2010).
- ⁹ J. Ahn, I. Hong, Y. Kwon, R. C. Clay, L. Shulenburger, H. Shin, and A. Benali, *Phys. Rev. B* **98**, 085429 (2018).
- ¹⁰ J. P. Hansen, *Phys. Rev. A* **8**, 3096 (1973).
- ¹¹ J. H. Chu and I. Lin, *Phys. Rev. Lett.* **72**, 4009 (1994).
- ¹² P. Drude, *Annalen der Physik* **319**, 667 (1904).
- ¹³ P. Drude, *Annalen der Physik* **319**, 936 (1904).
- ¹⁴ D. Cassidy, G. Holton, and J. Rutherford, “Understanding physics,” (Springer, New York City, 2002) Chap. 16.3, 1st ed.
- ¹⁵ We note that this quantity would not be sufficient to quantify whether a system is stable.
- ¹⁶ Note that higher-order (in)stabilities are, in all cases, weaker than at lower orders.
- ¹⁷ S. Mavadia, J. Goodwin, G. Stutter, S. Bharadia, D. Crick, D. M. Segal, and R. Thompson, *Nat. Commun.* **4**, 2571 (2013).
- ¹⁸ Throughout this paper, we use Hartree atomic units ($m_e = e = \hbar = k_e = 1$).
- ¹⁹ M. Bonitz, P. Ludwig, H. Baumgartner, C. Henning, A. Filinov, D. Block, O. Arp, A. Piel, S. Kding, Y. Ivanov, A. Melzer, H. Fehske, and V. Filinov, *Phys. Plasmas* **15**, 055704 (2008).
- ²⁰ E. Madelung, *Phys. Z.* **19**, 524 (1918).
- ²¹ E. Wigner, *Phys. Rev.* **46**, 1002 (1934).
- ²² E. Wigner, *Trans. Faraday Soc.* **34**, 678 (1938).
- ²³ J. R. Trail, M. D. Towler, and R. J. Needs, *Phys. Rev. B* **68**, 045107 (2003).
- ²⁴ J. Solanpaa, P. Luukko, and E. Räsänen, *J. Phys. Condens. Matter* **23** (2011).
- ²⁵ L. Bonsall and A. A. Maradudin, *Phys. Rev. B* **15**, 1959 (1977).
- ²⁶ P. G. Silvestrov and P. Recher, *Phys. Rev. B* **95**, 075438 (2017).
- ²⁷ M. Hinarejos, A. Prez, and M. C. Bauls, *New J. Phys.* **14**, 103009 (2012).
- ²⁸ R. A. Coldwell-Horsfall and A. A. Maradudin, *J. Math. Phys.* **1**, 395 (1960).
- ²⁹ W. J. Carr, *Phys. Rev.* **122**, 1437 (1961).
- ³⁰ G. Goldoni and F. M. Peeters, *Phys. Rev. B* **53**, 4591 (1996).
- ³¹ G. Goldoni, V. Schweigert, and F. Peeters, *Surf. Sci.* **361-362**, 163 (1996).
- ³² R. R. Palanichamy and K. Iyakutti, *Int. J. Quantum Chem.* **86**, 478 (2001).
- ³³ I. J. Zucker, *J. Phys. Condens. Matter* **3**, 2595 (1991).
- ³⁴ N. D. Drummond, Z. Radnai, J. R. Trail, M. D. Towler, and R. J. Needs, *Phys. Rev. B* **69**, 085116 (2004).
- ³⁵ X. Zhu and S. G. Louie, *Phys. Rev. B* **52**, 5863 (1995).
- ³⁶ D. M. Ceperley and B. J. Alder, *Phys. Rev. Lett.* **45**, 566 (1980).
- ³⁷ D. Ceperley, *Phys. Rev. B* **18**, 3126 (1978).
- ³⁸ L. Cândido, B. Bernu, and D. M. Ceperley, *Phys. Rev. B* **70**, 094413 (2004).
- ³⁹ G. Ortiz, M. Harris, and P. Ballone, *Phys. Rev. Lett.* **82**, 5317 (1999).
- ⁴⁰ S. Ciccariello, *Annal. Phys.* **18**, 157 (2009).
- ⁴¹ Y. Y. F. Liu, B. Andrews, and G. J. Conduit, *The Journal of Chemical Physics* **150**, 034104 (2019), <https://doi.org/10.1063/1.5070138>.
- ⁴² S. Ichimaru, *Rev. Mod. Phys.* **54**, 1017 (1982).
- ⁴³ D. H. E. Dubin and T. M. O’Neil, *Rev. Mod. Phys.* **71**, 87 (1999).
- ⁴⁴ Additionally, the successful quest to determine the intermediate physics arguably inspired the first application of importance-sampled diffusion Monte Carlo³⁶.
- ⁴⁵ R. W. Hasse and V. V. Avilov, *Phys. Rev. A* **44**, 4506 (1991).
- ⁴⁶ J. P. Schiffer, *Phys. Rev. Lett.* **88**, 205003 (2002).
- ⁴⁷ L. Hornekær, N. Kjærgaard, A. M. Thommesen, and M. Drewsen, *Phys. Rev. Lett.* **86**, 1994 (2001).
- ⁴⁸ R. C. Ashoori, *Nature* **379**, 413 (1996).
- ⁴⁹ Odd power terms in the potential trivially vanish due to symmetry.
- ⁵⁰ Throughout this paper, we normalize the particle mass such that $m = 1$.
- ⁵¹ S. Hamaguchi, R. T. Farouki, and D. H. E. Dubin, *Phys. Rev. E* **56**, 4671 (1997).
- ⁵² N. Greenwood and A. Earnshaw, *Chemistry of the Elements*, 2nd ed. (Elsevier, Amsterdam, Netherlands, 1997).
- ⁵³ C. Booth, E. Bauer, M. Maple, J. Lawrence, G. Kwei, and J. Sarrao, *J. Synchrotron Radiat.* **1**, 191 (2001).
- ⁵⁴ See Sec. SIII.
- ⁵⁵ C. Kittel, *Introduction to Solid State Physics*, 6th ed. (Wiley, Hoboken, U.S.A., 1986).
- ⁵⁶ B. Esther, *Basics Of Thermodynamics And Phase Transitions In Complex Intermetallics*, Vol. 1 (World Scientific, Singapore, 2008).
- ⁵⁷ W. A. Harrison, *Phys. Rev.* **118**, 1190 (1960).
- ⁵⁸ T.-S. Choy, J. Naset, J. Chen, S. Hershfield, and C. Stanton, *Bulletin of The American Physical Society* **45**, L36 42 (2000).

Supplementary Material: Absence of diagonal force constants in cubic Coulomb crystals

CONTENTS

I. Higher-order Derivative Test	1
II. Higher-order Matrices of Force Constants	2
III. Crystal Structures in the Periodic Table	2
IV. Numerical Model	3
A. Cubic systems (cub, bcc, fcc, dia)	3
B. Hexagonal systems (hcp, dhcp)	4
V. Details of the Tight-binding Model	5
A. Definitions	6
1. Wavefunction	6
2. Electron cloud potential and density	6
3. Ion potential and density	7
B. Ion-ion contribution	7
C. Electron-ion contribution	8
D. Electron-electron contribution	8
E. Pauli repulsion	8
F. Crystal relaxation	9
VI. Oscillatory Electron Density in the Nearly-free Electron Model	9
References	10

I. HIGHER-ORDER DERIVATIVE TEST

For a single-variable, real-valued and sufficiently differentiable function, f , let the first $(n - 1)$ derivatives vanish such that

$$f'(c) = \dots = f^{(n-1)}(c) = 0 \quad \text{and} \quad f^{(n)}(c) \neq 0,$$

where c is a constant in the domain of the function, and $n \in \mathbb{Z}^+$. In this case, the n th derivative may be used as a discriminant to determine the nature of the turning points.

If n is even:

- $f^{(n)}(c) < 0 \Rightarrow c$ is a local maximum,
- $f^{(n)}(c) > 0 \Rightarrow c$ is a local minimum.

If n is odd:

- $f^{(n)}(c) < 0 \Rightarrow c$ is a strictly decreasing point of inflection,
- $f^{(n)}(c) > 0 \Rightarrow c$ is a strictly increasing point of inflection.

Hence, this test can classify the critical points of f in all cases, provided $f^{(n)}(c) \neq 0$ for some value of n ^{S1}.

The higher-order derivative test may be generalized to multi-dimensional problems. Denoting $D^{(p)}f$ as the p th-order multivariate derivative of f , it can be shown that under corresponding conditions:

- $D^{(p)}f(c)$ is negative definite $\Rightarrow c$ is a strict local maximum.
- $D^{(p)}f(c)$ is positive definite $\Rightarrow c$ is a strict local minimum,
- $D^{(p)}f(c)$ is indefinite $\Rightarrow c$ is a saddle point,
- $D^{(p)}f(c)$ is zero or semidefinite \Rightarrow the test is inconclusive.

Note that, unlike the single-variable test, this test is not conclusive in all cases^{S2}.

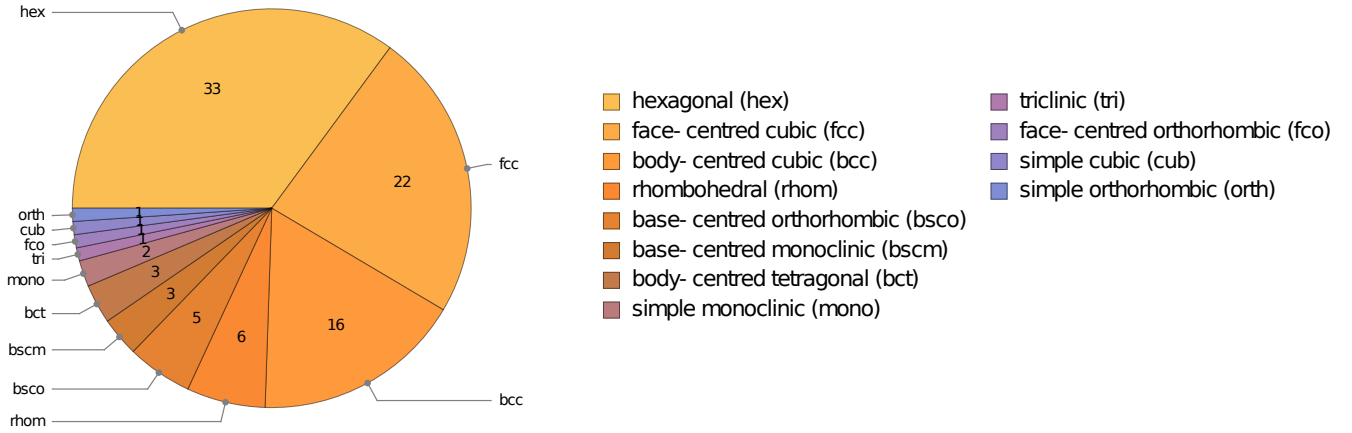


FIG. S1. Breakdown of crystal structures (by Bravais lattice) for the most thermodynamically stable allotropes of elements in the periodic table, at standard temperature and pressure. The number of elements exhibiting each crystal structure is given in the corresponding section of the chart. Crystal structure data is provided for an unambiguous subset containing 94 out of the 118 elements, using Mathematica’s ElementData function^{S3}.

II. HIGHER-ORDER MATRICES OF FORCE CONSTANTS

In this paper we consider the effect of displacing atoms originally at $\{\mathbf{R}_{Ii}^0\}$, on their nearest neighbors, with a total energy E and general displacements $\{\mathbf{R}_{Ii}\}$. We may expand the total energy such that:

$$\begin{aligned}
 E(\{\mathbf{R}_{Ii}\}) = & E(\{\mathbf{R}_{Ii}^0\}) + \sum_{Ii\alpha} \left. \frac{\partial E}{\partial u_{Ii\alpha}} \right|_{\mathbf{u}=0} u_{Ii\alpha} + \frac{1}{2!} \sum_{Ii\alpha} \sum_{Jj\beta} \Phi_{Ii\alpha, Jj\beta} u_{Ii\alpha} u_{Jj\beta} \\
 & + \frac{1}{3!} \sum_{Ii\alpha} \sum_{Jj\beta} \sum_{Kk\gamma} \left. \frac{\partial^3 E}{\partial u_{Ii\alpha} \partial u_{Jj\beta} \partial u_{Kk\gamma}} \right|_{\mathbf{u}=0} u_{Ii\alpha} u_{Jj\beta} u_{Kk\gamma} \\
 & + \frac{1}{4!} \sum_{Ii\alpha} \sum_{Jj\beta} \sum_{Kk\gamma} \sum_{Ll\delta} X_{Ii\alpha, Jj\beta, Kk\gamma, Ll\delta} u_{Ii\alpha} u_{Jj\beta} u_{Kk\gamma} u_{Ll\delta} + \dots,
 \end{aligned}$$

where $\{I, J, K, L\}$ are unit cell indices, $\{i, j, k, l\}$ are basis atom indices, and $\{\alpha, \beta, \gamma, \delta\}$ are Cartesian directions. As stated in the main text, translational invariance allows us to consider $\Phi_{Ii\alpha, 0j\beta}$ and $X_{Ii\alpha, 0j\beta, 0k\gamma, 0l\delta}$ without loss of generality. Furthermore, exploiting the symmetry of the system, we may additionally contract the fourth-order matrix of force constants such that $X_{Ii\alpha, 0j\beta, 0k\gamma, 0l\delta} \delta_\beta^\alpha \delta_\delta^\gamma = X_{Ii\alpha, 0j\alpha, 0k\gamma, 0l\gamma}$. Considering the diagonal force constant matrices then allows us to write these terms as $\Phi_I \equiv \Phi_{Ii\alpha, 0i\beta}$ and $\mathbf{X}_I \equiv X_{Ii\alpha, 0i\beta}$. Both of these matrices are symmetric.

III. CRYSTAL STRUCTURES IN THE PERIODIC TABLE

Sufficiently stable elements in the periodic table may be grouped in accordance with their crystal structure. A breakdown of the crystal structures (by Bravais lattice) in the periodic table is presented in Fig. S1. In the cases where an element exhibits multiple crystal structures at standard temperature and pressure, the most thermodynamically stable allotrope is given.

In three-dimensions, all crystal structures are derived from fourteen possible Bravais lattices. However, some of the derived crystal structures are worth studying separately, either due to their ubiquity (e.g. in the case of the hcp structure: the most common crystal structure in nature) or interesting properties (e.g. in the case of diamond). The cub, bcc, fcc, dia, hcp, and dhcp crystal structures are studied in particular in this paper because they only have one free parameter: the lattice constant. Furthermore, this group of crystal structures accounts for approximately three quarters of the known crystal structures in the periodic table.

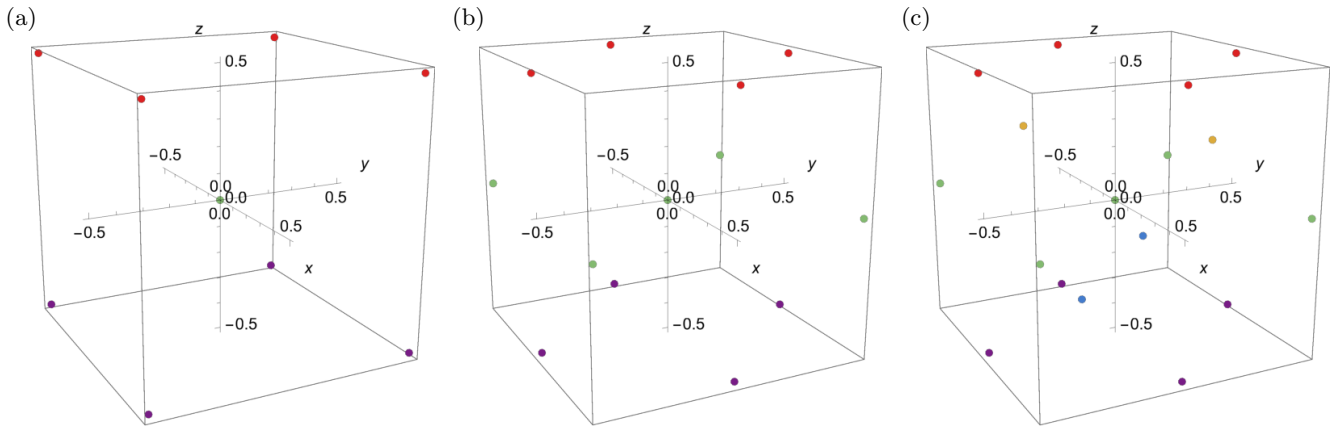


FIG. S2. Origin-centric unit cells for the (a) bcc, (b) fcc, and (c) dia, crystal structures. These structures have two, four, and eight atoms per unit cell, respectively. All lengths are given in units of the lattice constant, and the coloring distinguishes the position along the z -axis. The displacement vectors for these plots are given in Table S1a.

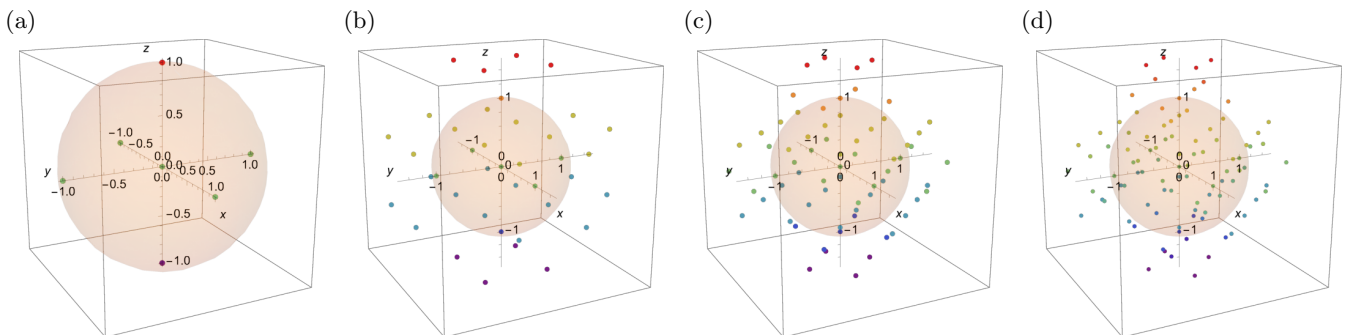


FIG. S3. Illustration of the points included in a one-shell summation of the (a) cub, (b) bcc, (c) fcc, and (d) dia, crystal structures. All points from the nearest-neighbor unit cells are considered. The centers of neighboring unit cells lie within a unit sphere (light orange). All lengths are given in units of the lattice constant, and the coloring of points distinguishes their position along the z -axis.

IV. NUMERICAL MODEL

In this section, we outline the numerical details of how the crystal structure summations were performed. In the interests of clarity, we use simplified notation in this section and consider the displacement of a single atom at the origin by a displacement vector \mathbf{R} .

A. Cubic systems (cub, bcc, fcc, dia)

In this paper, we consider unit cells with an atom situated at the origin in all cases. We refer to these as *origin-centric* unit cells, and we choose these in order to minimize finite system size error when summing radially outwards over many shells, as well as to simplify the computations. The unit cell for the simple cubic crystal consists of one atom situated at the origin. The unit cells for the bcc, fcc, and dia crystal lattices are shown in Fig. S2.

In order to sum to n shells, we include all atoms in units cells whose origins are situated within a radius of n lattice constants, as illustrated in Fig. S3. We continue to sum in this fashion until the properties of interest, such as the diagonal force constant matrices, converge to the desired precision.

The coordinates of the unit cell sites for these cubic systems is shown in Table S1a and the corresponding potentials are given in Table S1b. Hence, the summation over n shells may be written explicitly as

$$E_C = \sum_I V_C(\mathbf{R}_I - \mathbf{R}) = \sum_{i_x^2 + i_y^2 + i_z^2 \leq n^2} V_C \left(a \begin{pmatrix} i_x \\ i_y \\ i_z \end{pmatrix} - \begin{pmatrix} X \\ Y \\ Z \end{pmatrix} \right) - V \left(\begin{pmatrix} X \\ Y \\ Z \end{pmatrix} \right),$$

(a) Displacement Vectors

Crystal	Plane	Displacement Vectors of Sites in the Unit Cell
bcc	$z = a/2$	$\mathbf{r}_1^{\text{bcc}} = \frac{a}{2}(1, 1, 1), \mathbf{r}_2^{\text{bcc}} = \frac{a}{2}(-1, 1, 1), \mathbf{r}_3^{\text{bcc}} = \frac{a}{2}(1, -1, 1), \mathbf{r}_4^{\text{bcc}} = \frac{a}{2}(-1, -1, 1),$
	$z = -a/2$	$\mathbf{r}_5^{\text{bcc}} = \frac{a}{2}(1, 1, -1), \mathbf{r}_6^{\text{bcc}} = \frac{a}{2}(1, -1, -1), \mathbf{r}_7^{\text{bcc}} = \frac{a}{2}(-1, 1, -1), \mathbf{r}_8^{\text{bcc}} = \frac{a}{2}(-1, -1, -1)$
fcc	$z = 0$	$\mathbf{r}_1^{\text{fcc}} = \frac{a}{2}(1, 1, 0), \mathbf{r}_2^{\text{fcc}} = \frac{a}{2}(-1, 1, 0), \mathbf{r}_3^{\text{fcc}} = \frac{a}{2}(1, -1, 0), \mathbf{r}_4^{\text{fcc}} = \frac{a}{2}(-1, -1, 0),$
	$y = 0$	$\mathbf{r}_5^{\text{fcc}} = \frac{a}{2}(1, 0, 1), \mathbf{r}_6^{\text{fcc}} = \frac{a}{2}(-1, 0, 1), \mathbf{r}_7^{\text{fcc}} = \frac{a}{2}(1, 0, -1), \mathbf{r}_8^{\text{fcc}} = \frac{a}{2}(-1, 0, -1),$
	$x = 0$	$\mathbf{r}_9^{\text{fcc}} = \frac{a}{2}(0, 1, 1), \mathbf{r}_{10}^{\text{fcc}} = \frac{a}{2}(0, -1, 1), \mathbf{r}_{11}^{\text{fcc}} = \frac{a}{2}(0, 1, -1), \mathbf{r}_{12}^{\text{fcc}} = \frac{a}{2}(0, -1, -1)$
dia	$z = 0$	$\mathbf{r}_1^{\text{dia}} = \frac{a}{8}(4, 4, 0), \mathbf{r}_2^{\text{dia}} = \frac{a}{8}(-4, 4, 0), \mathbf{r}_3^{\text{dia}} = \frac{a}{8}(4, -4, 0), \mathbf{r}_4^{\text{dia}} = \frac{a}{8}(-4, -4, 0),$
	$y = 0$	$\mathbf{r}_5^{\text{dia}} = \frac{a}{8}(4, 0, 4), \mathbf{r}_6^{\text{dia}} = \frac{a}{8}(-4, 0, 4), \mathbf{r}_7^{\text{dia}} = \frac{a}{8}(4, 0, -4), \mathbf{r}_8^{\text{dia}} = \frac{a}{8}(-4, 0, -4),$
	$x = 0$	$\mathbf{r}_9^{\text{dia}} = \frac{a}{8}(0, 4, 4), \mathbf{r}_{10}^{\text{dia}} = \frac{a}{8}(0, -4, 4), \mathbf{r}_{11}^{\text{dia}} = \frac{a}{8}(0, 4, -4), \mathbf{r}_{12}^{\text{dia}} = \frac{a}{8}(0, -4, -4),$
	$z = a/4$	$\mathbf{r}_{13}^{\text{dia}} = \frac{a}{8}(2, 2, 2), \mathbf{r}_{14}^{\text{dia}} = \frac{a}{8}(-2, -2, 2),$
	$y = a/4$	$\mathbf{r}_{15}^{\text{dia}} = \frac{a}{8}(-2, 2, -2),$
	$x = a/4$	$\mathbf{r}_{16}^{\text{dia}} = \frac{a}{8}(2, -2, -2)$

(b) Potentials

crystal	atoms per unit cell	potential
bcc	2	$V_{\text{bcc}}(\mathbf{R}) = V(\mathbf{R}) + \frac{1}{8} \sum_{i=1}^8 V(\mathbf{R} + \mathbf{r}_i^{\text{bcc}})$
fcc	4	$V_{\text{fcc}}(\mathbf{R}) = V(\mathbf{R}) + \frac{1}{4} \sum_{i=1}^{12} V(\mathbf{R} + \mathbf{r}_i^{\text{fcc}})$
dia	8	$V_{\text{dia}}(\mathbf{R}) = V(\mathbf{R}) + \frac{1}{4} \sum_{i=1}^{12} V(\mathbf{R} + \mathbf{r}_i^{\text{dia}}) + \sum_{i=13}^{16} V(\mathbf{R} + \mathbf{r}_i^{\text{dia}})$

TABLE S1. (a) Displacement vectors for sites in a unit cell, and (b) corresponding unit cell potentials, for the bcc, fcc, and dia crystal structures. For the displacement vectors, the site at the origin is omitted and all vectors are given in terms of the lattice constant, a .

where $C \in \{\text{cub}, \text{bcc}, \text{fcc}, \text{dia}\}$ denotes the cubic crystal structure under consideration, and $\{i_x, i_y, i_z\}$ are integers. The summation yields the total potential energy of displacing the atom at the origin to a position \mathbf{R} . This expression can then be expanded to quadratic order in \mathbf{R} , for example, to extract the diagonal force constant matrix.

B. Hexagonal systems (hcp, dhcp)

Hexagonal systems are treated in an analogous fashion to cubic systems, except now more care is needed since the vectors to neighboring unit cells are not orthogonal. The origin-centric unit cells for the hcp and dhcp crystal lattices are shown in Figs. S4a & S4b and the corresponding displacement vectors and potentials are presented in Table S2. Hence for these systems, the (unnormalized) basis set, to go from one unit cell to another, may be denoted as

$$\{\mathbf{a}, \mathbf{b}, \mathbf{c}\} = \frac{a}{2} \left\{ \begin{pmatrix} 3 \\ -\sqrt{3} \\ 0 \end{pmatrix}, \begin{pmatrix} 3 \\ \sqrt{3} \\ 0 \end{pmatrix}, \begin{pmatrix} 0 \\ 0 \\ \frac{4\sqrt{6}}{3} \end{pmatrix} \right\},$$

where a is the lattice constant in the xy-plane. In this case, the summation over n shells may be explicitly written as

$$E_H = \sum_I V_H(\mathbf{R}_I - \mathbf{R}) = \sum_{\left(\frac{\sqrt{3}}{2}(i_x+i_y)\right)^2 + \left(\frac{i_y-i_x}{2}\right)^2 + i_z^2 \leq n^2} V_H \left(\frac{a}{2} \begin{pmatrix} 3(i_x+i_y) \\ \sqrt{3}(i_y-i_x) \\ \frac{4\sqrt{6}}{3}i_z \end{pmatrix} - \begin{pmatrix} X \\ Y \\ Z \end{pmatrix} \right) - V \left(\begin{pmatrix} X \\ Y \\ Z \end{pmatrix} \right),$$

where $H \in \{\text{hcp}, \text{dhcp}\}$ denotes the hexagonal crystal structure under consideration, and $\{i_x, i_y, i_z\}$ are integers. Figures S4c & S4d show the sites included in these summations up to eight shells, which is typically the number at which the desired precision converged. Note the approximate spherical symmetry of these systems.

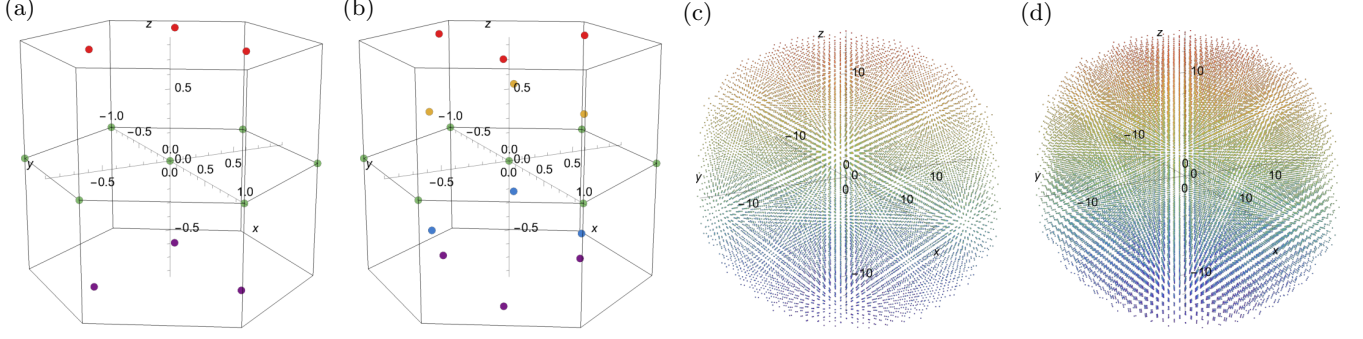


FIG. S4. [(a), (b)] Origin-centric unit cells for the (a) hcp, and (b) dhcp, crystal structures. These structures have six and twelve atoms per unit cell, respectively. [(c), (d)] Illustrations of the (c) hcp, and (d) dhcp, crystal structures plotted up to eight shells. All lengths are given in units of the lattice constant, and the coloring distinguishes the position along the z -axis. The displacement vectors for these plots are given in Table S2.

(a) Displacement Vectors

Crystal	Plane	Displacement Vectors of Sites in the Unit Cell
hcp	$z = 0$	$\mathbf{r}_1^{\text{hcp}} = a(1, 0, 0)$, $\mathbf{r}_2^{\text{hcp}} = \frac{a}{2}(1, \sqrt{3}, 0)$, $\mathbf{r}_3^{\text{hcp}} = \frac{a}{2}(-1, \sqrt{3}, 0)$, $\mathbf{r}_4^{\text{hcp}} = a(-1, 0, 0)$, $\mathbf{r}_5^{\text{hcp}} = \frac{a}{2}(-1, -\sqrt{3}, 0)$, $\mathbf{r}_6^{\text{hcp}} = \frac{a}{2}(1, -\sqrt{3}, 0)$,
	$z = 2\sqrt{6}/3$	$\mathbf{r}_7^{\text{hcp}} = \frac{a}{6}(3, \sqrt{3}, 2\sqrt{6})$, $\mathbf{r}_8^{\text{hcp}} = \frac{a}{6}(-3, \sqrt{3}, 2\sqrt{6})$, $\mathbf{r}_9^{\text{hcp}} = \frac{a}{3}(0, -\sqrt{3}, \sqrt{6})$,
	$z = -2\sqrt{6}/3$	$\mathbf{r}_{10}^{\text{hcp}} = \frac{a}{6}(3, \sqrt{3}, -2\sqrt{6})$, $\mathbf{r}_{11}^{\text{hcp}} = \frac{a}{6}(-3, \sqrt{3}, -2\sqrt{6})$, $\mathbf{r}_{12}^{\text{hcp}} = \frac{a}{3}(0, -\sqrt{3}, -\sqrt{6})$
dhcp	$z = 0$	$\mathbf{r}_1^{\text{dhcp}} = a(1, 0, 0)$, $\mathbf{r}_2^{\text{dhcp}} = \frac{a}{2}(1, \sqrt{3}, 0)$, $\mathbf{r}_3^{\text{dhcp}} = \frac{a}{2}(-1, \sqrt{3}, 0)$, $\mathbf{r}_4^{\text{dhcp}} = a(-1, 0, 0)$, $\mathbf{r}_5^{\text{dhcp}} = \frac{a}{2}(-1, -\sqrt{3}, 0)$, $\mathbf{r}_6^{\text{dhcp}} = \frac{a}{2}(1, -\sqrt{3}, 0)$,
	$z = \sqrt{6}/6$	$\mathbf{r}_7^{\text{dhcp}} = \frac{a}{6}(3, \sqrt{3}, \sqrt{6})$, $\mathbf{r}_8^{\text{dhcp}} = \frac{a}{6}(-3, \sqrt{3}, \sqrt{6})$, $\mathbf{r}_9^{\text{dhcp}} = \frac{a}{3}(0, -\sqrt{3}, \frac{\sqrt{6}}{2})$,
	$z = -\sqrt{6}/6$	$\mathbf{r}_{10}^{\text{dhcp}} = \frac{a}{6}(3, \sqrt{3}, -\sqrt{6})$, $\mathbf{r}_{11}^{\text{dhcp}} = \frac{a}{6}(-3, \sqrt{3}, -\sqrt{6})$, $\mathbf{r}_{12}^{\text{dhcp}} = \frac{a}{3}(0, -\sqrt{3}, -\frac{\sqrt{6}}{2})$,
	$z = \sqrt{6}/3$	$\mathbf{r}_{13}^{\text{dhcp}} = \frac{a}{6}(3, -\sqrt{3}, 2\sqrt{6})$, $\mathbf{r}_{14}^{\text{dhcp}} = \frac{a}{6}(-3, -\sqrt{3}, 2\sqrt{6})$, $\mathbf{r}_{15}^{\text{dhcp}} = \frac{a}{3}(0, \sqrt{3}, \sqrt{6})$,
	$z = -\sqrt{6}/3$	$\mathbf{r}_{16}^{\text{dhcp}} = \frac{a}{6}(3, -\sqrt{3}, -2\sqrt{6})$, $\mathbf{r}_{17}^{\text{dhcp}} = \frac{a}{6}(-3, -\sqrt{3}, -2\sqrt{6})$, $\mathbf{r}_{18}^{\text{dhcp}} = \frac{a}{3}(0, \sqrt{3}, -\sqrt{6})$

(b) Potentials

Crystal	Atoms per Unit Cell	Potential
hcp	6	$V_{\text{hcp}}(\mathbf{R}) = V(\mathbf{R}) + \frac{1}{3} \sum_{i=1}^6 V(\mathbf{R} + \mathbf{r}_i^{\text{hcp}}) + \frac{1}{2} \sum_{i=7}^{12} V(\mathbf{R} + \mathbf{r}_i^{\text{hcp}})$
dhcp	12	$V_{\text{dhcp}}(\mathbf{R}) = V(\mathbf{R}) + \frac{1}{3} \sum_{i=1}^6 V(\mathbf{R} + \mathbf{r}_i^{\text{dhcp}}) + \sum_{i=7}^{12} V(\mathbf{R} + \mathbf{r}_i^{\text{dhcp}}) + \frac{1}{2} \sum_{i=13}^{18} V(\mathbf{R} + \mathbf{r}_i^{\text{dhcp}})$

TABLE S2. (a) Displacement vectors for sites in a unit cell, and (b) corresponding unit cell potentials, for the hcp and dhcp crystal structures. For the displacement vectors, the site at the origin is omitted and all vectors are given in terms of the lattice constant, a .

V. DETAILS OF THE TIGHT-BINDING MODEL

In this section, we outline the details of the tight-binding configuration. As in Sec. IV, we use simplified notation for clarity. In our model, we have a crystal of ions with tightly-bound electrons at each site. We consider each atom to be composed of a pseudopotential, which takes into account the potential of the nucleus screened by the inner electrons, and one outermost electron.

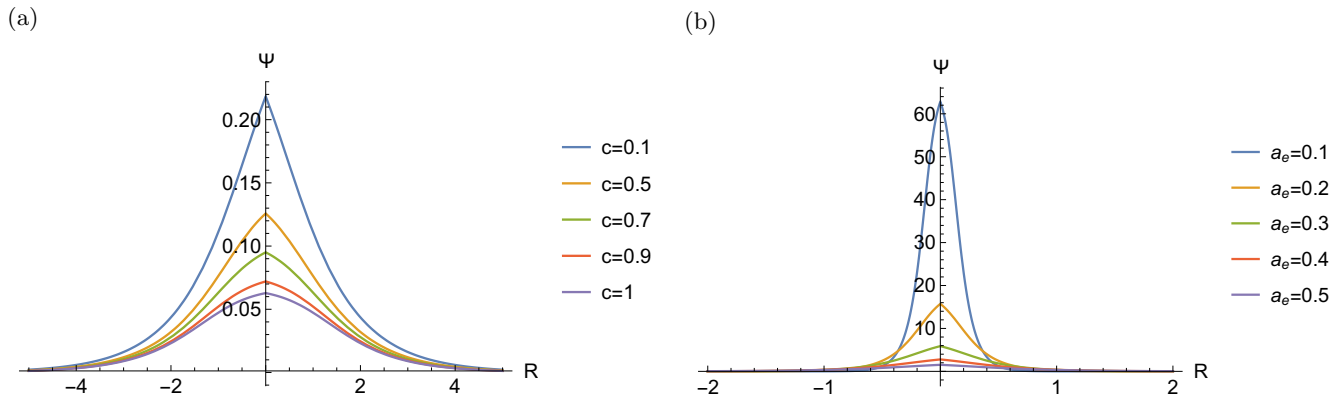


FIG. S5. Plots of the normalized wavefunction of the valence electron under the pseudopotential of the ion, Ψ . The behavior of the wavefunction is shown as we (a) vary c with $a_e = 1$, and (b) vary a_e with $c = 0.1$.

A. Definitions

1. Wavefunction

We start by taking an simplified ansatz for the wavefunction of the valence electron orbital under the potential of the ion:

$$\Psi(\mathbf{R}; c, a_e) = A \sqrt{\frac{1}{1 + \exp\left(\frac{2(|\mathbf{R}|-c)}{a_e}\right)}},$$

where A is a normalization constant, $a_e \ll R_I$ is the width of the valence electron cloud, and $0 \leq c < a_e$ is the width of the core electron cloud. We choose this ansatz so that the electron density is analytically well behaved in subsequent calculations, and that in the limit of vanishing radius and large distances we recover the wavefunction of a particle in a Dirac delta potential well:

$$\lim_{c \ll a_e \ll |\mathbf{R}|} \Psi \propto e^{-|\mathbf{R}|/a_e}. \quad (\text{S1})$$

This is the limit around which we will expand in the following sections. Plots of this wavefunction are shown in Fig. S5. Since it not possible to analytically derive an expression for the normalized wavefunction, we expand the probability density, $|\Psi|^2$ up to first order in the small parameter (c/a_e) and then solve the normalization condition $\int_{-\infty}^{\infty} |\Psi|^2 d\mathbf{R} = a_0/a_e$, where a_0 is the Bohr radius. This yields a normalization constant

$$A(c, a_e) = \frac{2\sqrt{a_0} (9a_e\zeta(3) - c\pi^2)}{9a_e^3\sqrt{3\pi}\zeta(3)^{3/2}} + O\left[\left(\frac{c}{a_e}\right)^2\right],$$

where $\zeta(3)$ is Apéry's constant.

2. Electron cloud potential and density

The valence electron cloud (which we denote using a capital 'E') has a potential given by the Coulomb potential of the single electron, $V_e(\mathbf{R}) = |\mathbf{R}|^{-1}$, integrated over the density distribution of the electron cloud:

$$V_E(\mathbf{R}; c, a_e) = \int V_e(\mathbf{R} + \mathbf{r}_e) \rho_E(\mathbf{r}_e; c, a_e) d\mathbf{r}_e,$$

where we calculate the density of the electron cloud using the normalized wavefunction defined in Sec. V A 1:

$$\rho_E(\mathbf{r}_e; c, a_e) = |\Psi(\mathbf{r}_e; c, a_e)|^2.$$

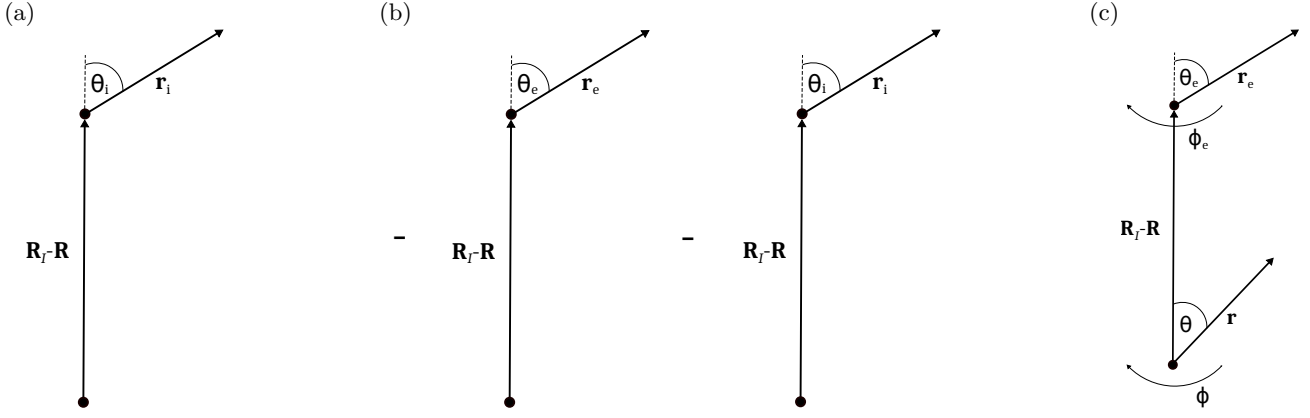


FIG. S6. Diagrams corresponding to the (a) ion-ion, (b) electron-ion, and (c) electron-electron contribution calculations. The displacement vector between ions, $\mathbf{R} - \mathbf{R}_I$, is oriented along the north pole, and the polar and azimuthal angles are defined in the range $0 \leq \theta < \pi$ and $0 \leq \phi < 2\pi$, respectively.

3. Ion potential and density

The ion potential is obtained by solving the time-independent Schrödinger equation and subtracting the energy constant, such that

$$V_i(\mathbf{R}; c, a_e) = -a_0 \left(\frac{1}{\Psi} \frac{\nabla^2}{2} \Psi - \lim_{|\mathbf{R}| \rightarrow \infty} \left(\frac{1}{\Psi} \frac{\nabla^2}{2} \Psi \right) \right).$$

The ion density is then subsequently obtained from Poisson's equation:

$$\rho_i(\mathbf{r}_i; c, a_e) = -\frac{\nabla^2 V_i(\mathbf{r}_i; c, a_e)}{4\pi}.$$

Note that due to the norm conserving property of our wavefunction ansatz, the ion density satisfies the normalization condition $\int_0^\infty \rho_i(r_i, c, a_e) 4\pi r_i^2 dr_i = a_0/a_e$ up to first order in (c/a_e) .

B. Ion-ion contribution

First, we calculate the repulsive potential felt by an ion at position \mathbf{R}_I due to an ion being displaced from the origin to a position \mathbf{R} . An illustration of the set-up is shown in Fig. S6a. Note that we orient the displacement vector between the two ions along the north pole to simplify the calculations. In order to calculate the ion-ion potential for the whole system we then sum over all distinct atoms, such that

$$E_{i-i}(\mathbf{R}; c, a_e) = \sum_I \int V_i(\mathbf{R}_I - \mathbf{R} + \mathbf{r}_i; c, a_e) \rho_i(\mathbf{r}_i; c, a_e) d\mathbf{r}_i.$$

Rewriting the ion potential in terms of the scalar variables defined in Fig. S6a, such that $V_i(|\mathbf{R}_I - \mathbf{R}|, \{r_i, \theta_i\}; c, a_e)$, we may Taylor expand the ion potential up to leading order in $(r_i/|\mathbf{R}_I - \mathbf{R}|)$:

$$\begin{aligned} E_{i-i}(\mathbf{R}; c, a_e) &= \sum_I V_i(|\mathbf{R}_I - \mathbf{R}|; c, a_e) \underbrace{\int \rho_i(\mathbf{r}_i; c, a_e) d\mathbf{r}_i}_{a_0/a} \\ &+ 2\pi \sum_I \int_{r_i=0}^\infty \int_{\theta_i=0}^\pi \left(\frac{\partial^2 V_i}{\partial r_i^2} \right) r_i^4 \rho_i(r_i; c, a_e) \sin(\theta_i) d\theta_i dr_i + O \left[\left(\frac{r_i}{|\mathbf{R}_I - \mathbf{R}|} \right)^3 \right]. \end{aligned}$$

Note that the first-order term in the expansion vanishes by symmetry. Hence the final expression for the ion-ion contribution is derived accurate to first order in (c/a_e) and second order in $(r_i/|\mathbf{R}_I - \mathbf{R}|)$. Taken together, this forms the leading-order analytical expansion about the tight-binding limit introduced in Sec. VA 1.

C. Electron-ion contribution

The next contribution is that due to the electron-ion interaction. There are attractive potentials felt by the electron cloud due to the ions, as well as those felt by the ion due to the electron clouds. A sketch of this scenario is shown in Fig. S6b, where the minus signs indicate that this is an attractive interaction. As in the previous section, we set up the general form of the electron-ion contribution as

$$E_{e-i}(\mathbf{R}; c, a_e) = - \sum_I \int V_i(\mathbf{R}_I - \mathbf{R} + \mathbf{r}_e; c, a_e) \rho_E(\mathbf{r}_e; c, a_e) d\mathbf{r}_e - \sum_I \int V_E(\mathbf{R}_I - \mathbf{R} + \mathbf{r}_i; c, a_e) \rho_i(\mathbf{r}_i; c, a_e) d\mathbf{r}_i.$$

It can be shown, either by symmetry or integration by parts, that this expression reduces to

$$E_{e-i}(\mathbf{R}; c, a_e) = -2 \sum_I \int V_i(\mathbf{R}_I - \mathbf{R} + \mathbf{r}_e; c, a_e) \rho_E(\mathbf{r}_e; c, a_e) d\mathbf{r}_e.$$

Rewriting the ion potential in terms of scalar variables, as before, we may Taylor expand up to leading order in $(r_e/|\mathbf{R}_I - \mathbf{R}|)$:

$$\begin{aligned} E_{e-i}(\mathbf{R}; c, a_e) &= -2 \sum_I V_i(|\mathbf{R}_I - \mathbf{R}|; c, a_e) \underbrace{\int \rho_E(\mathbf{r}_e; c, a_e) d\mathbf{r}_e}_{a_0/a} \\ &\quad - 4\pi \sum_I \int_{r_e=0}^{\infty} \int_{\theta_e=0}^{\pi} \left(\frac{\partial^2 V_i}{\partial r_e^2} \right) r_e^4 \rho_E(r_e; c, a_e) \sin(\theta_e) d\theta_e dr_e + O \left[\left(\frac{r_e}{|\mathbf{R}_I - \mathbf{R}|} \right)^3 \right]. \end{aligned}$$

Analogously to before, the electron-ion contribution is derived to first order in (c/a_e) and second order in $(r_e/|\mathbf{R}_I - \mathbf{R}|)$, which is the leading-order analytical expansion about the tight-binding limit in this model.

D. Electron-electron contribution

Finally, we compute the repulsive electron-electron contribution to the potential. Again the displacement vector between the ions is aligned along the north pole. The valence electrons are parameterized in spherical polar coordinates around each atom, as depicted in Fig. S6c. The electron-electron contribution in this case may be written as

$$E_{e-e}(\mathbf{R}; c, a_e) = \sum_I \iint V_e(\mathbf{R}_I - \mathbf{R} + \mathbf{r}_e - \mathbf{r}) \rho_E(\mathbf{r}_e; c, a_e) \rho_E(\mathbf{r}; c, a_e) d\mathbf{r}_e d\mathbf{r}.$$

Due to the spherical symmetry of each electron cloud, this contribution reduces exactly to Coulomb repulsion, such that

$$E_{e-e}(\mathbf{R}; a_e) = \frac{a_0^2}{a_e^2} \sum_I \frac{1}{|\mathbf{R}_I - \mathbf{R}|}.$$

Note the total potential energy of the system at this stage, $E_{i-i} + E_{e-i} + E_{e-e}$, tends to zero as $(c/a_e) \rightarrow 0$ and $|\mathbf{R}| \gg a_e$. In this limit, the electrons are effectively on top of the ions and the whole system is neutral due to Gauss' theorem.

E. Pauli repulsion

To complement our result for the energy, we estimate the Pauli repulsion felt by the overlapping electron clouds. Since we only consider spherically symmetric (i.e. s-type) orbitals in the toy model, this reduces to a one-dimensional problem. We consider a Dirac delta potential well, of depth g , inside an infinite square well, such that:

$$V_{\text{well}}(x) = \begin{cases} -g\delta(x), & |x| = 0, \\ 0, & 0 < |x| < L, \\ \infty, & |x| \geq L. \end{cases}$$

In this scenario, g determines how tightly bound the electrons are to their respective atoms, and L represents the effective radius for the electron clouds. As L is reduced, the bound state energy is increased – this represents the energy increase due to the Pauli repulsion of overlapping orbitals.

The wavefunction takes the form $\Psi \propto \sinh(k(L - |x|))$ inside the infinite well, where k is the wave number. Considering the derivative continuity of the wavefunction at the origin, we derive the transcendental equation $\tanh y = \chi y$, where we have defined $y \equiv kL$ and $\chi \equiv \hbar^2/mgL$. We can derive an analytical form for the solution, and hence the scaling behavior of the energy with L , by finding the lowest root with a Newton-Raphson scheme. The iterative equation for the root is then

$$y_{n+1} = y_n - \frac{\tanh y_n - y_n \chi}{\operatorname{sech}^2 y_n - \chi},$$

where $n \in \mathbb{Z}^+$. Since we are interested in the regime where the wavefunction is significantly influenced by the boundary wall, we take y_n to be small. Additionally, we are interested in the limit when Pauli repulsion is dominant i.e. when L is small. Taking these limits together, we find that $y_\infty = \sqrt{3\chi/2}$. Hence the energy of the bound state is

$$E_{\text{Pauli}} = \frac{\hbar^2}{2mL^2} y_\infty^2 = \frac{3\hbar^2}{4m^{3/2}\sqrt{2E_b}L^3},$$

where we define the binding energy of an isolated Dirac delta potential well as $E_b \equiv mg^2/2\hbar^2$. In the tight binding approximation, the wavefunction takes the form $\Psi \propto \exp(-m^{1/2}\sqrt{2E_b}L/\hbar)$. Comparing this to the form of the wavefunction in Eq. S1 allows us to make the identification $E_b \sim a_e^{-2}$ up to physical constants. Hence, in atomic units, the energy gain due to Pauli repulsion becomes

$$E_{\text{Pauli}} = \frac{3a_e}{4L^3}.$$

Note that due to the differences in unit cell geometry, the lattice constant cannot be directly compared between the various crystal structures. For this, we may examine the optimal effective radius of each atom in a spherical packing, defined as

$$r_{\text{eff}} = \left(\frac{3}{4\pi} \frac{V_{\text{unit cell}}}{N_{\text{unit cell}}} \right)^{1/3},$$

where $V_{\text{unit cell}}$ is the optimal volume of the unit cell, and $N_{\text{unit cell}}$ is the number of atoms enclosed. In place of L , we evaluate E_{Pauli} at the effective optimum radius. This rudimentary approximation for the Pauli repulsion allows us to analytically capture the scaling behavior as the lattice constant is reduced.

F. Crystal relaxation

Let us define the total energy of the system as

$$E(\mathbf{R}; c, a_e) = E_{i-i}(\mathbf{R}; c, a_e) + E_{e-i}(\mathbf{R}; c, a_e) + E_{e-e}(\mathbf{R}; a_e) + E_{\text{Pauli}}(a, a_e).$$

Note that there is an implicit lattice constant dependence in the first three terms in the form of the potentials, as well as in the lattice summations. Once we have calculated an analytical form for the total energy of the system as a function of the displacement of the central atom, \mathbf{R} , and implicitly the lattice constant, a , we then compute the optimal lattice constant such that:

$$a_{\min} = \operatorname{argmin}_{a \in (a_e, \infty)} (E).$$

We subsequently relax the system to this lattice constant and re-evaluate the total energy at a given \mathbf{R} . This renders the total energy as a function of c and a_e only.

VI. OSCILLATORY ELECTRON DENSITY IN THE NEARLY-FREE ELECTRON MODEL

In order to approximate the oscillatory part of the electron cloud density in the nearly-free electron model, we consider Fourier transforms of the reciprocal lattices, as shown in Table S3. For crystals with a single-atom basis,

Crystal	$\rho_E^{\text{osc}}(\mathbf{r})/u$
cub/bcc/fcc	$\frac{1}{\tilde{N}_{\text{c.s.}}} \sum_{i=1}^{\tilde{N}_{\text{c.s.}}} \cos(\mathbf{r} \cdot \tilde{\mathbf{r}}_i^{\text{c.s.}})$
dia	$\frac{1}{8} \left[\sum_{i=1}^8 \cos(\mathbf{r} \cdot \tilde{\mathbf{r}}_i^{\text{dia}}) + \sum_{i=1}^8 \cos\left(\left(\mathbf{r} - \mathbf{r}_{13}^{\text{dia}}\right) \cdot \tilde{\mathbf{r}}_i^{\text{dia}}\right) \right]$
hcp	$\frac{A_{\text{hcp}}}{6} \left[\sum_{i=1}^6 \cos(\mathbf{r} \cdot \tilde{\mathbf{r}}_i^{\text{hcp}}) \cos\left(\frac{3\pi}{\sqrt{6}a} z\right) + \sum_{i=1}^6 \cos\left(\left(\mathbf{r} - \mathbf{r}_7^{\text{hcp}}\right) \cdot \tilde{\mathbf{r}}_i^{\text{hcp}}\right) \cos\left(\frac{3\pi}{\sqrt{6}a} \left(z - \frac{\sqrt{6}a}{3}\right)\right) \right]$
dhcp	$\frac{1}{6} \left[\frac{1}{3} \sum_{i=1}^6 \cos(\mathbf{r} \cdot \tilde{\mathbf{r}}_i^{\text{dhcp}}) \cos\left(\frac{3\pi}{\sqrt{6}a} z\right) + \sum_{i=1}^6 \cos\left(\left(\mathbf{r} - \mathbf{r}_7^{\text{dhcp}}\right) \cdot \tilde{\mathbf{r}}_i^{\text{dhcp}}\right) \cos\left(\frac{\sqrt{6}\pi}{a} \left(z - \frac{a}{\sqrt{6}}\right)\right) \right]$
	$+ \frac{1}{3} \sum_{i=1}^6 \cos\left(\left(\mathbf{r} - \mathbf{r}_{14}^{\text{dhcp}}\right) \cdot \tilde{\mathbf{r}}_i^{\text{dhcp}}\right) \cos\left(\frac{3\pi}{\sqrt{6}a} \left(z - \frac{\sqrt{6}a}{3}\right)\right) \right]$

TABLE S3. Oscillatory part of the electron cloud density in the nearly-free electron model, ρ_E^{osc} , in units of the oscillation strength, u . $\tilde{N}_{\text{c.s.}}$ is the number of displacement vectors, and $\{\tilde{\mathbf{r}}_i^{\text{c.s.}}\}$ the set of displacements, in a unit cell of the reciprocal lattice. The vectors $\mathbf{r}_i^{\text{c.s.}}$ are defined in Tables S1 and S2. The normalization constant, $A_{\text{hcp}} = 2/3$, is chosen such that $\max\{\rho_E^{\text{osc}}\} = u$ for all crystal structures.

the resulting function has a simple form. However, for crystals with more than one atom in the basis, we consider a superposition of multiple offset lattices^{S4}; with modulation along the z-axis, where appropriate. The functions, ρ_E^{osc} , are scaled such that $\max\{\rho_E^{\text{osc}}\} = u$ for all crystal structures. Over a unit cell, all of the functions integrate to zero.

[S1] E. Gkioulekas, *Int. J. Sci. Math. Educ.* **45**, 118 (2014).

[S2] M. A. H. Nerenberg, *Int. J. Sci. Math. Educ.* **22**, 303 (1991).

[S3] W. R. Inc., “Mathematica, Version 11.3,” (2018).

[S4] Note that the offsets given in Table S3 are not unique.